UNIVERSITY OF CALIFORNIA

SANTA CRUZ

THERMOPLASMONIC PHOTOINACTIVATION OF *VIBRIO CHOLERAE*

A thesis submitted in partial satisfaction
of the requirements for the degree of

MASTER OF SCIENCE

in

ELECTRICAL ENGINEERING

by

Mingran Liu

December 2018

The Thesis of Mingran Liu
is approved:

_____
Professor Ahmet Ali Yanik, Chair

_____
Professor Sung-Mo "Steve" Kang

_____
Professor Nobuhiko P. Kobayashi

_____
Lori Kletzer
Vice Provost and Dean of Graduate Studies

Table of Contents

List of Figures

List of Tables

Abstract

THERMOPLASMONIC E PHOTOINACTIVATION OF *VIBRIO CHOLERAE*

by

Mingran Liu

Vibrio Cholerae is considered an important human pathogen causing worldwide health problem and commonly exists in aquatic reservoirs. Photoinactivation of 405 nm light and photothermal disinfection by near infrared lasers have been investigated on various types of bacterial species with a notably high killing efficien. This work combines the photoinactivation of 405 nm light with plasmonic enhanced photothermal effect on the surface of an Al nanoantenna disk array. A significant cell reduction of *Vibrio Cholerae* was found after 20 min illumination with almost 99.99% of bacteria inactivated which suggests potential use for clinical and medical applications.

Acknowledgments

This takes me back to the days when I was in UCSC. I would like to thank Professor Ahmet Ali Yanik for giving me opportunities and so much guidance on this project. Without his help I never would have finished this great research. Many Thanks to Professor Nobuhiko Kobayashi for teaching me how to be independent and resourceful.

I am grateful to work with all lab members in the Nanoengineering Group and NECTAR Lab at UCSC. Especially, I would like to thank Jude, for monitoring my project and teaching me how to be a qualified researcher in the past year and David Fryauf, who gave me brilliant suggestions for solving problems. I really learnt a lot from their rigorous academic attitude. Special thanks to the members of the reading committee: Professor Yu Zhang and Professor Sung-Mo “Steve” Kang for supporting this work. I would like to thank Michael in Fitnat’s group for biological support, Dr. Tom Yuzvinsky for SEM imaging and Neil for reviewing my thesis.

Thermoplasmonic Pathogen Inactivation of 405 nm Light: Combining Photodynamics with Photothermal Effect

1. Introduction

Vibrio Cholerae, a gram-negative comma-shaped human pathogen, usually infects aquatic reservoirs and water supply[1-4]. It causes watery diarrhea by secreting a toxin once it colonizes in the intestine. It causes a fast progressing infection that is often fatal due to dehydration from severe diarrhea[5, 6]. Researchers have estimated that roughly four million people are infected by vibrio cholerae annually and about 120,000 people die from related infections every year[7]. During 2016, 132,121 cholerae cases from 38 different countries were reported to World Health Organization[8] (WHO). Vibrio cholerae is a global threat to public health, and there is an urgent need for development of disinfection techniques.

An effective way to control micro-organism including bacteria and pathogens is thermal inactivation through protein denaturation in cell structures. Previous studies have observed ceased cell reproduction and roughened cell morphology of Staphylococcus epidermidis bacteria at 60 ℃ on a Peltier plate[9]. Comparing the temperature treatments at 37 and 45 ℃, a 100-fold higher cell colony reduction has

been observed[9]. Irradiation of infrared light (IR) or near-infrared light (NIR) can deliver heat by triggering a molecular transition to a higher vibrational energy level. Reported studies have demonstrated thermal inactivation of bacteria in root canals[10-12] using near-infrared (975 nm) laser irradiation. However, particularly high laser powers on the order magnitude of a million watts per square centimeter are needed to achieve approximately 30 ℃ temperature elevation [10]. As for photothermal inactivation of vibrio cholera, there is no study reported in literature. One study has demonstrated a 95.5% decrease in bacteria count after growing the bacteria at 47 ℃ for 10 min compared to growing them at 30 ℃ [13]. Even when the growing temperature was reduced to 42 ℃, an approximately 90% decrease in bacteria count was still observed. These results suggest that vibrio cholerae is extremely sensitive to temperature, and less heat would be required to attain similar thermal inactivation efficiencies compared to the other bacteria species[7, 9, 14]. Photothermal effect based thermal inactivation could be a very efficient and effective approach in the disinfection of vibrio cholera. Since less heat may be needed, this would reduce the illumination light intensity even further relative to the intensity used in [ref 10-12]. Hence, it might not be necessary to use a laser for the inactivation of vibrio cholera as less light intensity would be needed. Lasers are not ideal for heat generation since they could raise safety concerns for the users such as causing severe or permanent skin or eye injuries. This especially true for infrared laser that emits invisible radiation, which causes sluggish 'eye aversion response' putting users at higher risk for eye damage. Furthermore, it requires precise optical alignment, focusing, or collimation components and laser

stabilization systems, making it less adaptable for practical applications or field use. In contrast, light-emitting diodes (LED) pose significantly less potential harm, while power output of LEDs could be sufficient for thermal inactivation purposes when combined with thermoplasmonic heat generation. Another feasibility provided by LED is that small sized LED can always be well-prepackaged without any associated optics, which allows for a more flexible fixture design than laser could offer. More importantly, LED distributes power more evenly and maintain power more stably over a larger exposure area compared to lasers that requires stabilization systems and optics to concentrate power in a tiny focused region. Therefore, LED could be an alternative light source for heat generation that is well suited for thermal inactivation/sterilization of bacteria with a minimal amount of energy required.

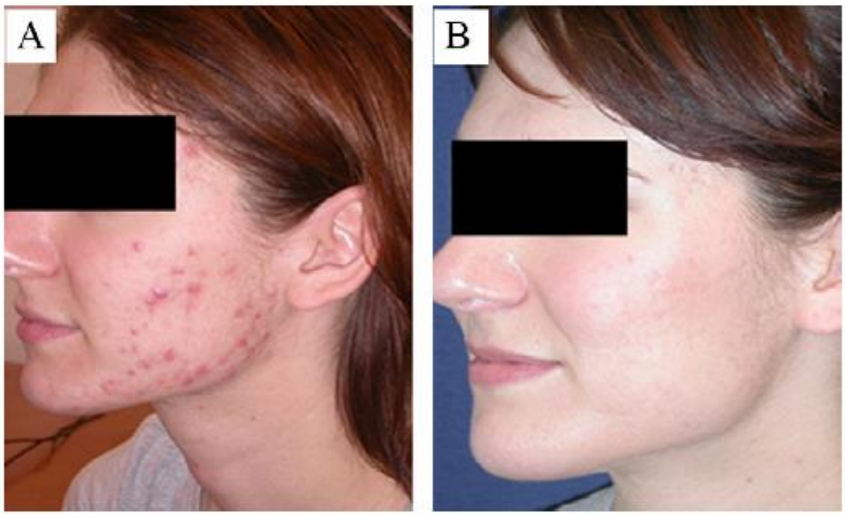

Figure 1: The Wellman Center for Photomedicine utilized blue light with 407 ~ 420 nm wavelength for acne treatment: (A) before and (B) after blue light illumination [15]

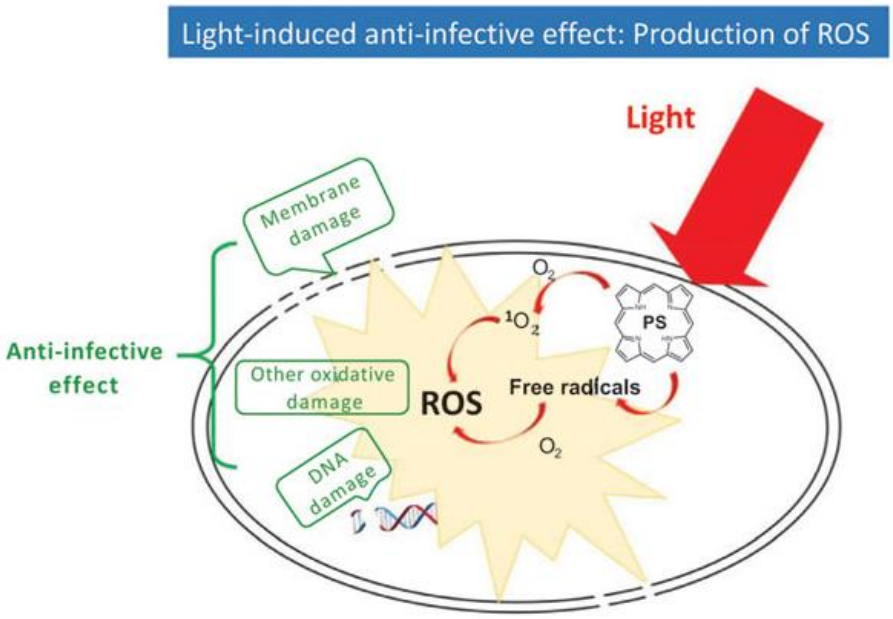

Figure 2: Inactivation kinetics of ROS in microorganisms[16]

Pathogen inactivation of blue light has recently attracted wide attention due to its broad therapeutic application and antimicrobial efficacy[17]. The Wellman Center for Photomedicine at Massachusetts General Hospital utilized photoinactivation with blue light (407 ~ 420 nm) for acne treatment by illuminating blue light directly on a patient's face. As a result of this illumination, a marked clinical improvement was observed before and after the treatment shown in Fig. 1[15]. Moreover, few studies have also reported that efficacy and effectiveness of using blue light in photo-inactivating pathogens such as Propionibacterium acnes on face (407 ~ 420 nm) [18-20], Helicobacter pylori in stomach (405 ~ 408 nm) [21-23] and different types of oral bacterial species (400 ~ 500 nm) [24, 25]. The antibacterial mechanism of blue light

was investigated and recent studies discovered that blue light actually induces oxygen-dependent photo-excitation of porphyrins in exposed micro-organisms[15, 26, 27]. The generated porphyrins react with oxygen or cell components, producing reactive oxygen species (ROS) through a photodynamic process. The produced ROS causes oxidative damage to the cell membrane by disrupting cytoplasmic content and cell walls[27]. Recent work[28] has demonstrated that blue light around 400 ~ 500 nm wavelength inhibited reproduction of aggregates of Streptococcus mutans bacteria cells by the photo-excited ROS, an 80% reduction in cell population was observed after 10 min exposure at an intensity of 11.4 mW/mm^2. Although the blue light used in this paper is effective in generating ROS to induce a significant biocidal effect on microbial cells, antimicrobial blue light (aBL) within a certain wavelength is limited for use in occupied environments as it poses a serious light exposure associated hazard for human health[27, 29]. However, in the regions of 440 and 480 nm, blue light causes side effects on human health associated with photoretinitis and influences mood and circadian rhythms[27]. In contrast, 405 nm, a particular wavelength of violet-blue light, is well below the wavelength of blue light and above the wavelength of ultraviolet. 405 nm light not only has no adverse impact on human body, but also shows significantly antimicrobial efficacy against a wide range of bacterial pathogens[15, 26, 27] (Fig. 2 from ref. 24). Researchers have demonstrated that the illumination of 405 nm light on Staphylococcus aureus bacteria for 7.5 hours resulted in approximately 87% reduction in bacteria population with about 0.2 mW/mm^2 light irradiance[30]. However, such exposure

times are impractically long. The antimicrobial efficacy could be enhanced if thermal and photonic inactivation mechanisms are integrated.

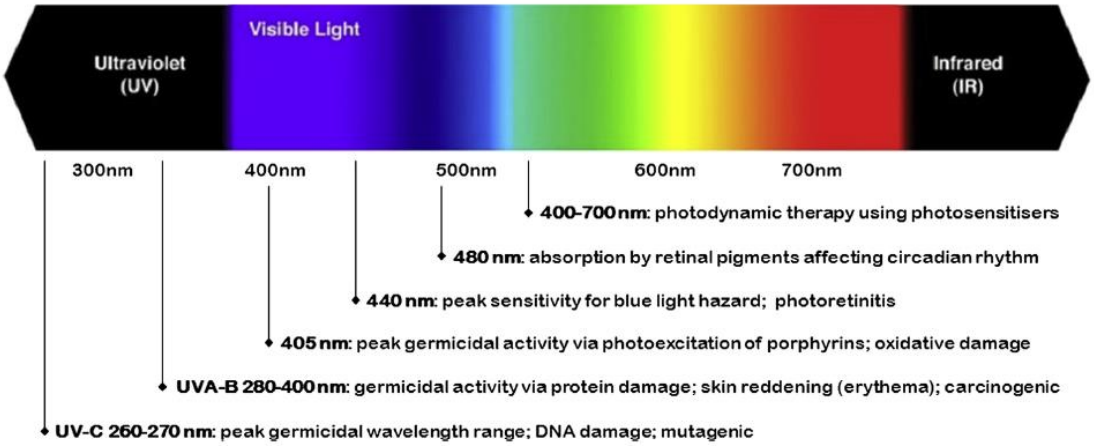

Figure 3: Electromagnetic spectrum of the light, the highlighted regions are the critical wavelengths with antibacterial effect and corresponding safety issues[27]

Metal nanoparticles are capable of generating heat efficiently in the presence of electromagnetic radiation[31]. Typically, this process becomes significantly enhanced in the regime of plasmon resonance since the heat generated inside the nanostructure is correlated with light absorption, which leads to a strong localized heating in metallic nanoparticles[32]. Shape and organization of nanoparticles also contributes to plasmonic resonant photothermal heat generation as recent studies demonstrated. For instance, a specific structure of diabolo antenna was designed and revealed higher heating efficiency than a normal complementary bow-tie antenna due to Babinet's principle[33]. Moreover, localized heating in confined volumes yields high local temperature in the regime of certain designed plasmonic nanostructure such as nanocrystal trimer[34] and four-member homogeneous quadrumer[35]. More

importantly, these studies suggest that heat generation can be further improved by engineering the nanoparticle structure in a matrix, especially in the regime of continuous-wave (CW) illumination, since the heat generation process also involves resonant coupling into plasmon modes besides absorption of incident photons[31]. Instead of localizing heat generation within a single nanostructure, plasmonic resonant heating in a nanoparticle array is of particular interest in recent studies and shows a more optimized thermal effect [36, 37].

In this study, the photothermal inactivation of vibrio cholerae using 405 nm LEDs on an Al nanoantennae array was investigated and compared with the efficacy on a conventional glass slide. Our nanoplasmonic device showed a significant photothermal efficacy of almost 100% on an Al nanoantennae array after only 10 min illumination. This revolutionary design constructs a novel nano-photonic and nano-photothermal therapy against vibrio cholera, promising for antibacterial treatment and more potential applications.

2. Experimental Setup and Method

2.1 Chamber Design

A cylindrical chamber was designed in order to load bacterial suspension for light exposure. The chamber was assembled by sandwiching a slide between two acrylic slabs and tightening with screws on four corners of the slabs. A circular hole (area of the circle 285 mm^2) was cut through the middle of two slabs for two purposes: (1) the

upper slab creates a volume of approximately 1.38 mL for the chamber (2) the lower slab yields an optical path for exposing light directly on bottom of the slide. In particular, this chamber doesn't contain any lids for closure with the purpose of pipetting accessibility. In addition, a homemade enclosure was prepared for supporting the chamber and a circular area of 285 mm^2 was made in order to create an optical path for light exposure.

2.2 405 nm LED

The high-intensity narrow-spectrum (HINS) 405 nm Solis™ LED system (Thorlabs Inc, Newton, NJ, USA) consists of an array of 12 individual LEDs in a matrix (arrangement of LEDs is shown in Fig. 4) was utilized for illumination of bacteria. The system emits violet-blue light with a peak output at 405 nm (spectrum is shown in Fig. 4) with 14 nm bandwidth at full-width half-maximum (FWHM). The power (3.1 ~ 7.1 W) of the LED can be tuned using an LED driver with six fixed scale bars. The irradiances of the LED with respect to these six different power levels were measured and calculated at a distance of approximately 3 cm (the distance between the slide and LED) using an optical power meter (Thorlabs Inc, Newton, NJ, USA) and listed in Table 1. A maximum irradiance of 2.5 mW/mm^2 was used for exposure of bacteria. This LED includes a collimation optics in a lens tube with a large clear aperture Ø48.3 mm (Ø1.90″), which is much larger than the radius (9.525 mm) of custom-designed and manufactured chamber. The normalized intensity of the LED between ± 9.525 mm is shown (Fig. 4). This LED features passive cooling instead of an internal fan in order to eliminate vibrations that would normally degrade exposure quality in the experiment.

Each diode is mounted to a heatsink inside of a 127.8 mm × 127.8 mm × 162.0 mm vented housing to efficiently dissipate heat.

Table 1: Optical Irradiance of 405 nm LED

Scale	1	2	3	4	5	6	7	8
Irradiance (mW/mm^2)	2.5	2.064	1.185	0.665	0.2925	0.135	0.0525	0.01

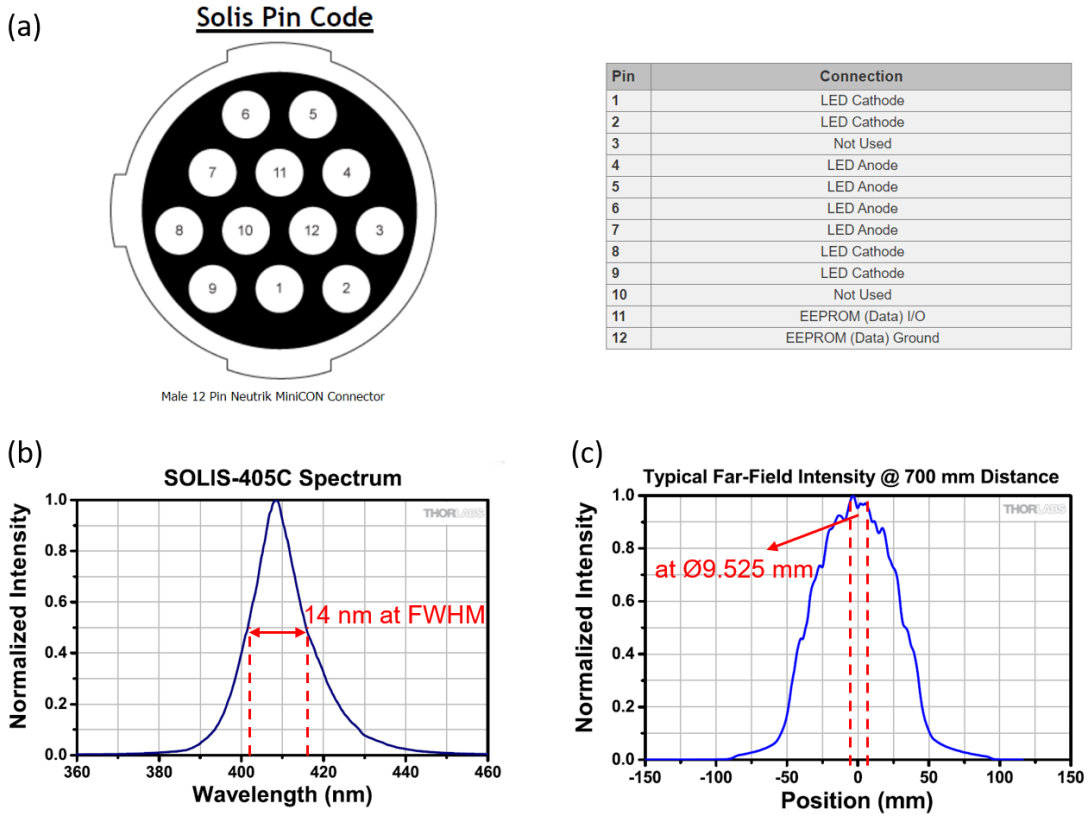

Figure 4: (a) arrangement of LEDs (b) spectral width of LED (c) typical far field intensity of LED

2.3 Numerical Simulation

The optical and thermal simulations were carried out using Lumerical's FDTD solutions and DEVICE (Lumerical, Inc.). The periodic boundary conditions are in the x and y directions. The incident beam is set to propagate through the positive z-direction. The scaling factor in the heat source was set to 605, which corresponds to the optical input power (irradiance × area) of 605 mW in the FDTD simulation. The convective boundary condition of nanoantenna array in DEVICE was defined as the interface of water and Al in order to model the heat loss at the top of the surface through convection.

2.4 SEM Imaging of Bacterial Morphology

Sample fixation was performed by immersion in 3% glutaraldehyde buffered with 0.1M (1X) PBS at room temperature for 1 hour. Samples were then washed twice in DI water for 10 s followed by air dry rinse. A graded ethanol solution (25%, 50%, 75%, 90%, 100%, 100%) was employed for serial dehydration over 10 min. Critical point drying (CPD) was carried out for 1 hour.

2.5 Live/Dead Imaging

Using the BacLight Live/Dead kit, a mixture of equal parts component A and component B were mixed thoroughly, and 3 µL were added per 1 mL of DASW to make a diluted dye solution. After light exposure the DASW buffer in the chamber was discarded. The slide was removed from the chamber and 350 µL of the dye solution was gently pipetted onto the slide and incubated at room temperature in the dark for 30

minutes. The dye droplet was manipulated to cover the attached bacterial region of the slide. Following this, the dye solution was removed, and the slide was submerged five times in DASW. One drop of mounting oil was placed on the slide, and then covered by a coverslip. Images were taken on UCSC Microscopy Facility's ZEISS Axioimager using the GFP fluorescent channel for the SYTO9 dye and the mCherry fluorescent channel for the propidium iodide.

3. Bacterial Cell Recovery Test

In order to figure out the best way to collect bacteria from the surface after a 1 hour attachment, we investigated the recovery methodology for our experimental use and two experimental tests were performed. Firstly, pipetting time for recovery was investigated. An overnight culture (GFP-tagged strains) was diluted 1/100 into 2% LB and 1 mL of this bacterial suspension was pipetted into the chamber for a 1 hour incubation at room temperature in the dark. Subsequently, the supernatant bacterial liquid was aspirated and the chamber was gently washed by PBS twice. Following the gentle wash, the chamber was refilled with 1 mL of PBS followed by aggressive pipetting to detach all the cells from the surface. Different pipetting times were set as 30, 60 and 90 seconds for comparison. A cross-sectional pattern was utilized in order to pipette the entire surface of the recovery area. The recovered bacterial liquid was then serially diluted in PBS and track plated on LB agar plates in triplicate. The

supernatant bacterial liquid and the liquid of the second gentle wash were also serially diluted and track plated. Enumeration of the surviving bacterial cells was accomplished by manually counting viable colonies on the plate. The results from the Table 2 show that 90 seconds of PBS pipetting detached more cells than those of 30 and 60 seconds. Although there are around $6.0x10^5$ CFU's in the second wash, compared to the results of PBS pipetting, there is a 2 orders of magnitude difference in CFU's. Therefore, the PBS gentle wash before aggressive pipetting shouldn't have impact on quantifying surface-attached cells.

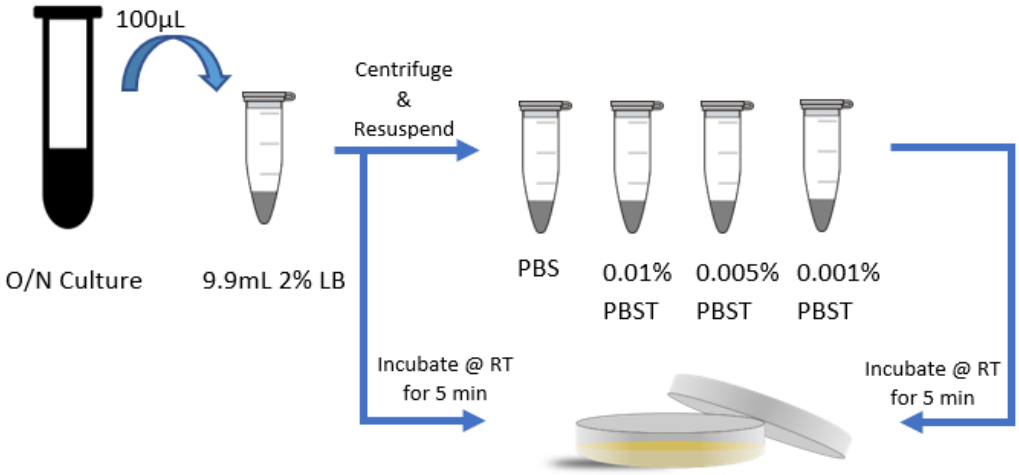

Figure 5: Illustration of pipetting time experimental protocol

The recovered slides were observed by fluorescence microscopy for tracking the remaining GFP-tagged bacterial cells on the surface after aggressive pipetting. As shown in Figure 6, the remaining bacteria cells are dramatically decreased following 30 s pipetting. However, there is no such significant change in 60 and 90 s pipetting.

This suggests that 90 s pipetting is sufficient for the bacterial cell recovery and can be applied in our illumination experiment.

Table 2: List of bacterial recovery results

	Supernatant	**Second wash**	**30 secs of pipetting**	**60 secs of pipetting**	**90 secs of pipetting**
CFU/mL	$1.0\text{-}2.0\times10^{7}$	6.0×10^{5}	1.0×10^{7}	1.3×10^{7}	1.65×10^{7}

Table 3: List of results of different concentration of PBST

	Source	**Initial**	**PBS**	**0.01% PBST**	**0.005% PBST**	**0.001% PBST**
CFU/mL	3.9×10^{9}	1.47×10^{7}	1.13×10^{7}	1.13×10^{7}	1.08×10^{7}	9.6×10^{6}

In order to investigate the detachment effect associated with detergent, PBS and its mixture with Tween-20 of various concentrations (so-called PBST) were employed for pipetting. Three different concentrations of 0.001%, 0.005% and 0.01%(v/v) Tween-20 were added into 1 mL PBS respectively and followed the same recovery procedure as above for 90 s pipetting. The 2% LB diluted culture was mixed with either PBS or PBST in order to test if Tween-20 affects viability of *V. cholerae*. The results in the Table 3 suggest that Tween-20 aids removing cells from the surface as increasing Tween-20 concentration improves the recovery of cells. However, we've found that

there is a significant cell loss when Tween-20 is used. Tween-20 adversely impacts cell viability of *V. cholerae*. Hence, we decided to use 90 seconds of pipetting with PBS for viable cell recovery from the surface.

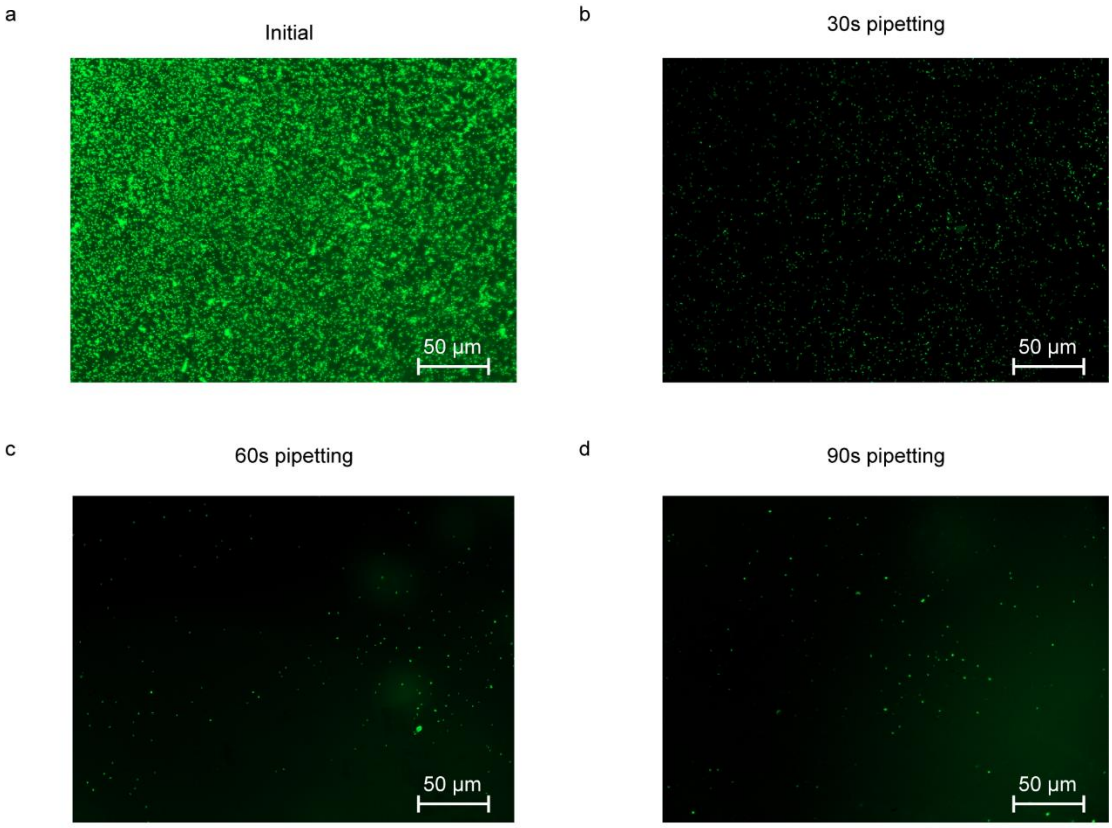

Figure 6: The fluorescence imaging of the surface with initial bacteria and after (a) 30, (b) 60 and (c) 90 s pipetting

Table 4: List of results of Tween-20 viability test

	2% LB without 0.01% Tween 20	**2% LB with 0.01% Tween 20**
CFU/mL	2.23×10^7	1.6×10^7

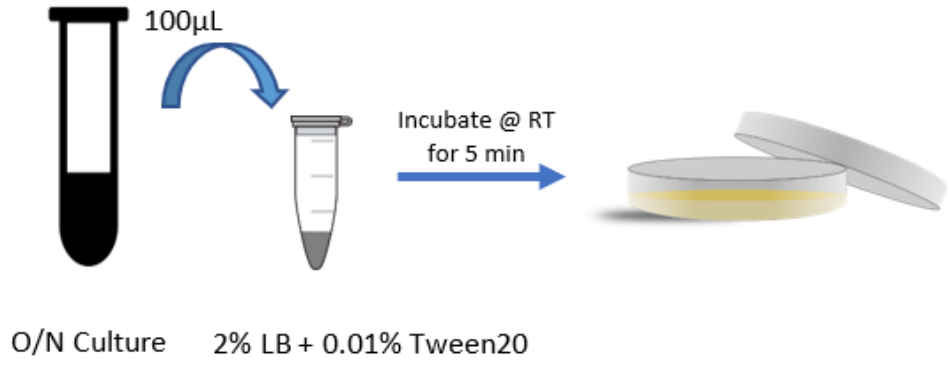

Figure 7: Illustration of Tween-20 viability test

4. Simulation and Characterization Results of Thermoplasmonics

To investigate the optimization of photothermal properties of Al nanoantenna disk array, steady-state temperature profile induced by 405 nm continuous-wave (CW) illumination was simulated. At first, the optical absorption was analyzed by FDTD Solutions (Lumerical, Inc.). The incident light beam was set at the bottom of the nanoantenna array propagating through the glass and optically excited Al nanoantenna under the heating beam with 2.5 mW/mm^2 irradiance. The total input power was subsequently scaled as 1 mW for the entire array while the input power for a single nanoantenna was acquired by the scaled input power 1 mW divided by the number of nanoantennas in the region of illuminated area. This area was considered circular with a diameter of 19.05 mm. The incident beam was focused on this area, resulting in nanoantennas being heated in this vicinity. Then the temperature increase induced by

the optical absorption was calculated by thermal modeling in DEVICE (Lumerical, Inc.). To take the collective effect into account, the scaling factor of the heat source was set to 605 which corresponds to the optical input power (irradiance × area) of 605 mW in the FDTD simulation. The convective boundary condition of nanoantenna array was defined as the interface of water and Al in order to model the heat loss at the top of the surface through convection. The temperature profile was calculated and mapped for different Al nanoantennas with various radius (24 to 48 nm) and periodicities (300 to 202 nm). The results of the thermal simulation show that the nanoantenna yields a significant temperature increase of 46 ℃ with a radius of 34 nm with 262 nm periodicity in the array. This establishes our design rationale as the strongest optical absorption and photothermal conversion occurs in the plasmonic structures with dramatically suppressed radiative losses. For nanoantenna arrays without optimized radiative couplings, radiative losses lead to diminished photothermal heat generation as shown in Figure 8. Following a series of FDTD simulations and analytical analysis, we demonstrated that the maximum heat generation occurs at 405 nm for structures with 34 nm radius and 262 nm periodicity.

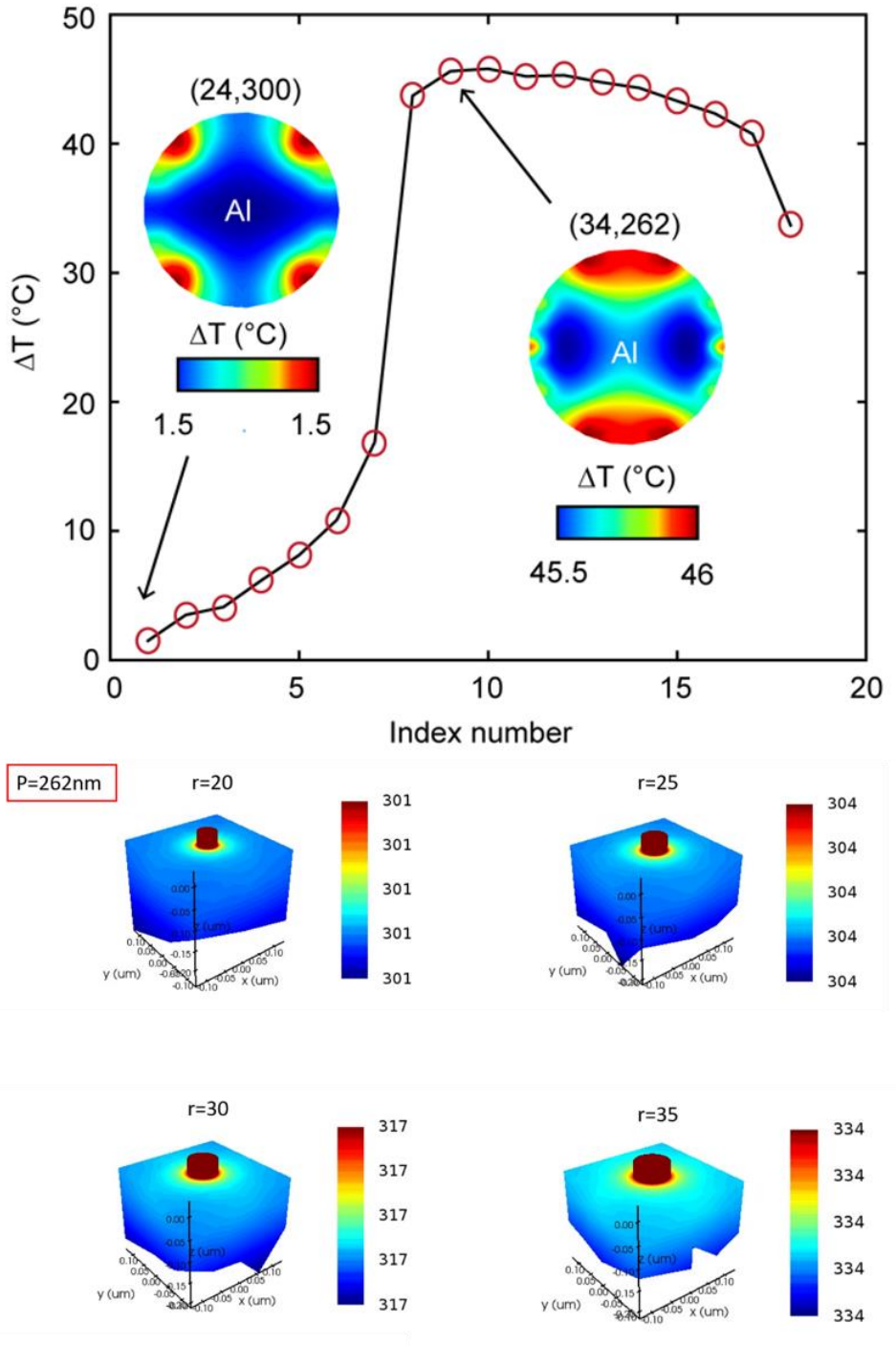

Figure 8: The FDTD and DEVICE simulation of Al nanoantenna array. The optimal heat generation occurs at r=34 nm and p=262 nm

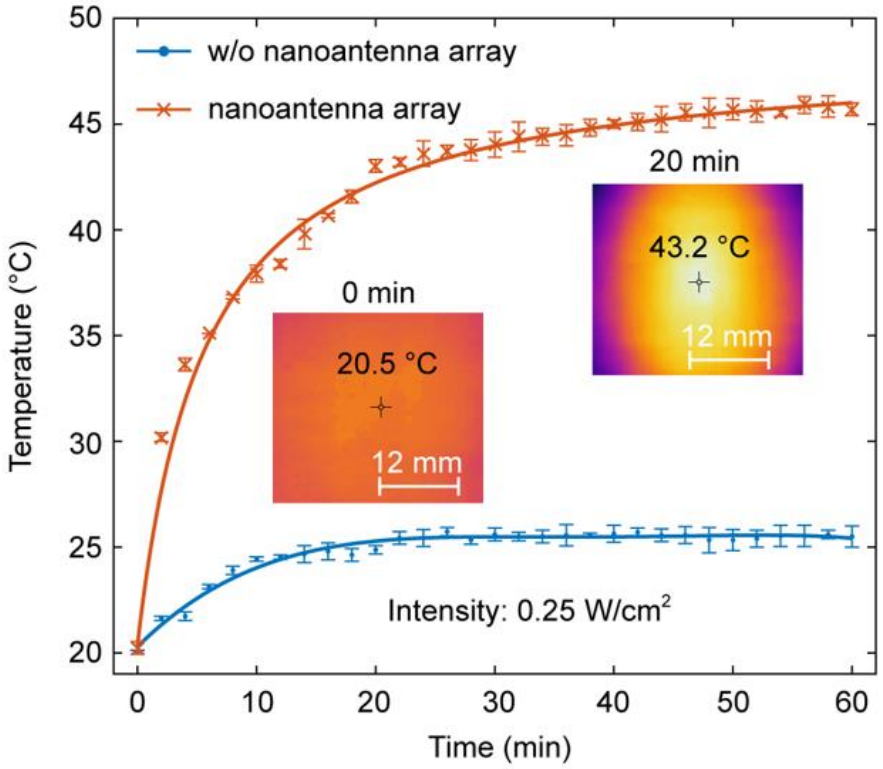

Figure 9: Experimental temperature measurement using thermal camera on the surface of bare glass (blue line) and nanoantenna array (red line)

Following our FDTD analysis, we experimentally determined the photothermal property of Al nanoantenna disk array with 405 nm illumination. The thermal probing of an optimized nanoantenna array slide was performed to assess the temperature elevation in response to the time increase and was compared to the performance of a normal glass slide. To do so, a high-intensity narrow-spectrum (HINS) 405 nm Solis™ LED system (Thorlabs, Inc., Newton, NJ, USA) consisting of an array of 12 individual LEDs in a matrix was utilized for illumination. This system emits violet-blue light at a peak output of 405 nm (irradiance = 0.25W/cm^2) with a 14 nm bandwidth at full-width

half-maximum (FWHM). For exposure, the sample slide was positioned above the LED system at a distance of approximately 3 cm on a homemade exposure platform. 1.3 mL volume of Deionized (DI) water was subsequently dropped by a syringe directly on the surface of the sample slide so it could be held within an area of about 1 × 1 inches due to the surface tension. Then the sample slides were exposed and optically heated with continuous-wave (CW) illumination with irradiance of $0.25 W/cm^2$ for 60 min in total. The heat transfer from the irradiated sample slides to surrounding media (DI water) was evaluated by measuring temperature on the surface of the slides using FLIR One (FLIR® Systems, Inc.) thermal camera at intervals of 2 min. A significant temperature enhancement of about 25 ℃ compared to pre-exposure condition of room temperature 20 ℃ is found in nanoantenna array slides as shown in Figure 10. This temperature elevation stems from thermoplasmonic contribution of plasmonic nanoantenna and non-radiative decay processes in the presence of reduced radiative losses in the illuminated region. Our experimental measurements validate our proposed localized surface plasmonic resonances (LSPRs) design rationale. In comparison with a normal glass slide, we observed that the nanoantenna array requires a prolonged time (approximately 50 min) to reach the steady state condition, a clear indication of enhanced heat generation requiring longer time span to reach thermal equilibrium of with the ambient through heat dissipation. While normal glass slides take only 20 min to reach thermal equilibrium. As a result of enhanced heat generation, nanoantenna arrays shows a dramatic temperature increase within the 10 mins. In fact, almost 10 ℃ of temperature increase within only 2 min exposure is observed. We observed

temperatures as high as 38.2 ℃ within 10 mins. This indicates strong nanoplasmonic heat generation that might be exploited for bacterial photothermal inactivation.

5. Evolution of Temperature Increase with Power

Temperature measurements of nanoantenna arrays and bare glass slides under various heating beam powers were performed using the same thermal probing methodology and setup in Figure 9. The slides were optically heated with eight different LED powers from 2.4 mW to 605 mW and the temperature was monitored with a FLIR One (FLIR® Systems, Inc.) thermal camera after 20 min illumination. The resulting temperature versus different heating beam powers were recorded in Figure 10. Under an LED intensity of 2.5 mW/mm^2, linear dependence between temperature and power results in a temperature increase of 5.2 ℃ and 23.13 ℃ on bare glass slides and nanoantenna array slides, respectively. The significant temperature changes on the surface of nanoantenna array with respect to glass surface experimentally validates our proposed design rationale which demonstrates that the current density in the nanoantenna array generates much more heat than bare glass.

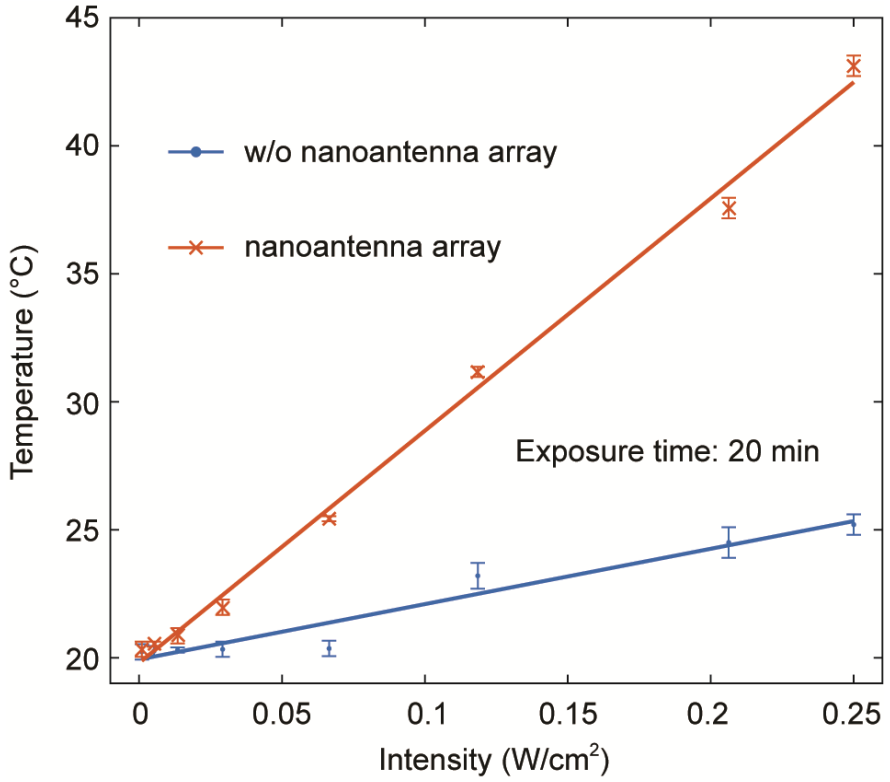

Figure 10: Evolution of temperature increase versus LED power

6. Bacterial Inactivation Efficiency

In order to verify the antimicrobial capability of nanoantenna disk array illumination on *V. cholerae*, the cell viability assay was performed to assess the inactivation efficiency of nanoantenna array slides after 405 nm exposure and compared to bare glass slides. For experimental use, O1 El Tor A1552 *V. cholerae* (wild type) were grown aerobically in Luria-Bertani (LB) broth (1% tryptone, 0.5% yeast extract, 1% NaCl, pH 7.5) at 30°C. LB agar contained granulated agar (Difco) at 1.5% (wt/vol). Defined artificial seawater was used in place of PBS during the live/dead imaging.[38]

Over the course of bacterial attachment, overnight *V. cholerae* liquid culture, inoculated from five single colonies, were diluted 1/100 in 2% LB (0.02% tryptone, 0.01% yeast extract, 1% NaCl, pH 7.5) and 1 mL of the diluted sample was pipetted into the preassembled homemade glass slide chambers. These chambers contained either a bare glass slide or a nanoantenna array slide. *V. cholerae* was then attached to the surface for one-hour incubation in the dark. We selected one hour for attachment as this has been proven to be an adequate time for an irreversible surface attachment of a single monolayer bacteria [39]. 2% LB was employed to minimize cell growth as previously done [40, 41]. Following attachment, the bacterial liquid was removed to avoid bacteria reattachment and the chamber was gently washed with either PBS (bacterial recovery) or DASW (live/dead imaging). The chamber was refilled with the appropriate buffer to provide aquatic condition for bacteria and positioned above the LED using the same exposure platform we stated before. Subsequently, the chamber was exposed to 405 nm LED (irradiance = 2.5mW/mm^2) for different duration times 5 (75 J/cm^2), 10 (150 J/cm^2) and 20 min (300 J/cm^2) respectively. Following light exposure, the PBS buffer in the chamber was pipetted aggressively for 90 s to detach the all cells from the surface. Cross-sectional patterns were used to evenly agitate the surface of the slide. The recovered bacterial liquid was then serially diluted in PBS and track plated on LB agar plates in triplicate. The 1/100 diluted cell culture and the bacterial liquid without subsequent light exposure were also serially diluted and track plated. Enumeration of surviving colonies was performed the following day by manually counting colony-forming units (CFU) on agar plate.

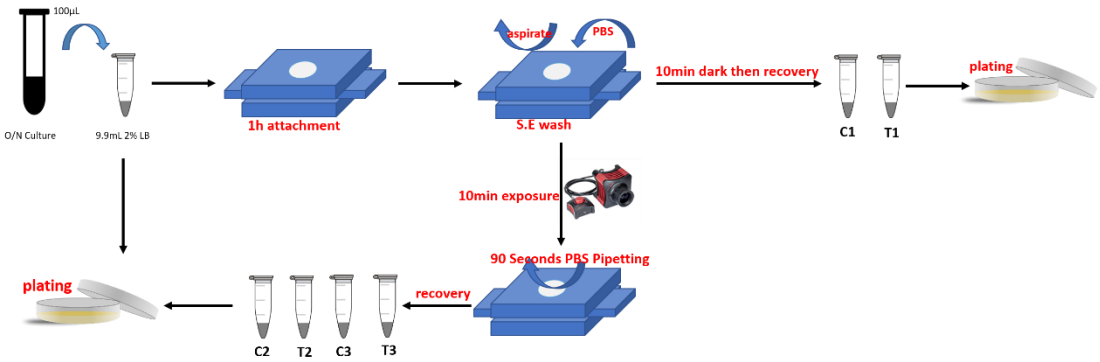

Figure 11: Illustration of 405 nm LED exposure protocol, where T represents treatment which means the surface is designed as nanoantenna array, C donates as control which means the use of bare glass surface

Enumeration results have demonstrated a significant photothermal inactivation of *V. cholerae* on nanoantenna array by 405 nm illumination. A remarkable bacterial reduction of 4.5 $\log_{10}$ CFU mL^{-1} was achieved in nanoantenna array slides following 20 min exposure. This results in 99.99% of bacterial cells inactivated by a localized surface temperature of 43.2 ℃ induced by the enhanced surface plasmonic resonant heat. In contrast, in experiments performed on bare glass slide, we only observed 0.5, 1.0 and 1.9 $\log_{10}$ CFU mL^{-1} cell reductions after 5, 10, and 20 min illumination, respectively. Similar cell reduction was also exhibited in nanoantenna array slide from 0 min to 5 min and could be explained with oxidative cellular damage by reactive oxygen species (ROS) generated through a photodynamic process in bacterial organisms [15, 26, 27]. This process was also mentioned in previous studies for various bacteria species [24, 30, 42, 43]. By combining the photoinactive and photothermal effects, our design rational shows a more rapid inactivation of almost 4.5 $\log_{10}$ CFU

mL^{-1} reduction of bacterial cells killed within only 20 min. This evidence validates our plasmonic enhanced heat generation profile in the course of 10 to 20 min as the temperature varies from 38.2 to 43.2 ℃, which is lethally high for *V. cholerae*.

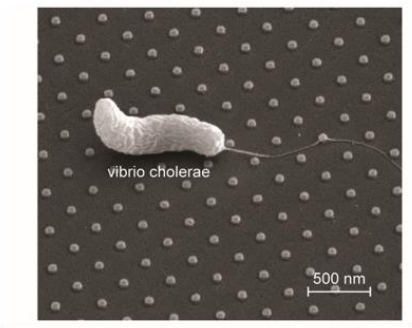

Figure 12: SEM imaging of *V. Cholerae* on our designed Al nanoantenna array

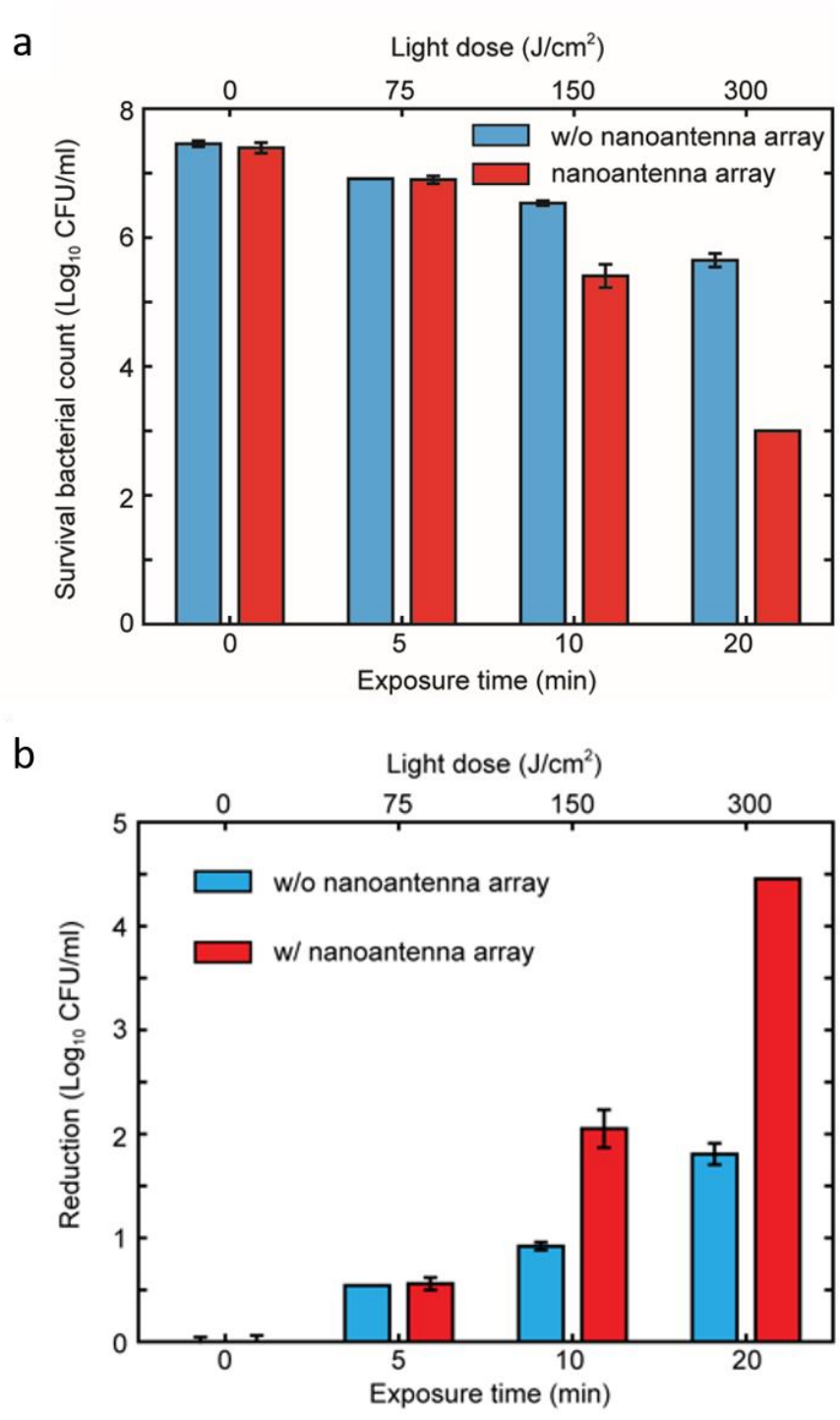

Figure 13: Killing efficiency of 405 nm on glass (blue bar) and nanoantenna array (red bar) surface. (a) survival bacterial count (b) bacterial cell reduction

The inactivation behavior and bacterial susceptibility on the surface of glass and nanoantenna array were analyzed using a modified Weibull model.[30, 44-46] Based on this statistical approach, the survival rate of bacteria is described as the number of surviving bacteria at a specific light dose (irradiance × exposure time), *N*, divided by the number of initial bacteria colonies, N_0. In this case, the bacterial inactivation kinetics can be described using the following equation and satisfy a Weibull distribution:

$$\log_{10}\left(\frac{N}{N_0}\right) = -0.4343\left(\frac{t}{\alpha}\right)^{\beta} \quad (1)$$

where the scale parameter α correlates to the antibacterial times associated with the bacterial population and was considered to indicate the bacterial resistance as a response to the increased light dose. Coefficient β is the shape parameter and determines the shape of Weibull distribution, which suggests the germicidal timeliness of illumination depend on the light dose. For nanoantenna array surface, the value of β is larger than 1 (β = 2) during the first 10 min exposure indicating an accumulated bacterial inactivation rate with an increase in the light dose. This can be explained by the elevated temperature from approximately 33 to 38.2 ℃ in the period of 5 to 10 min. At this point, the physiological state of *V. cholerae* was adversely impacted as the temperature increase and the viability was dramatically decreased as 1.5 $\log_{10}$ CFU mL^{-1}. However, only a 0.5 $\log_{10}$ CFU mL^{-1} reduction was achieved over 5 min in absence of the photothermal effect. On the other hand, in the case that β is smaller than 1 (β = 0.893), the rate of inactivation gradually decreases as an increasing light dose which

indicates a much higher inactivation rate at a lower light dose. This is exhibited by the cell reduction from 5 (7 $\log_{10}$ CFU mL^{-1}) to 20 min (3 $\log_{10}$ CFU mL^{-1}) where a lower killing rate was obtained from 10 to 20 min compared to 5 to 10 min. The increased temperature from 10 to 20 min may potentially inactivate the bacteria associated with a heat resistance. In contrast, the value of β in bare glass slide is nearly 1 suggesting that the pure 405 nm photoinactivation of *V. cholerae* on bare glass surface is not dose-dependent. There was nearly a 0.5 $\log_{10}$ CFU mL^{-1} reduction on glass slide every 5 min due to the exposure of 405 nm LED. This indicates that photoinactivation behavior of 405 nm for *V. cholerae* shows a relatively lower germicidal efficiency compared to that of photothermal inactivation and one can potentially upgrade the killing efficiency by combining the photoinactivation with photothermal effect. Live/Dead imaging shows a significant antibacterial effect on the surface of Al nanoantenna array after 20 min illumination. The green color and red color represents surviving cells and dead cells, respectively.

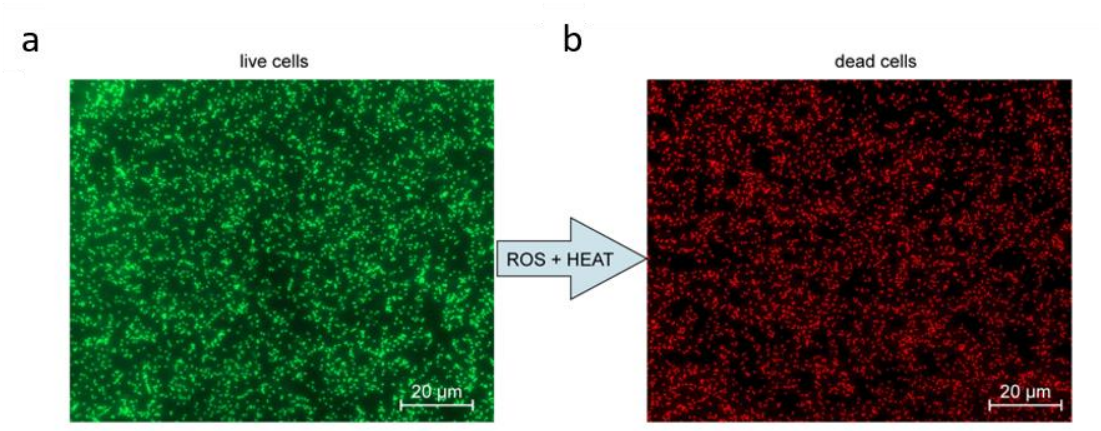

Figure 14: Live/Dead imaging (a) before and (b) after 20 min 405 nm exposure

7. Conclusion

A remarkable photothermal inactivation was achieved in nanoantenna array slides following 20 min exposure resulting in 4.5 $\log_{10}$ CFU mL^{-1} bacterial cell reduction based on enumeration. According to the bacterial counting, 99.99% of bacterial cells were inactivated after 20 min exposure by a localized surface temperature of 43.2 ℃ induced by the surface plasmonic enhanced heat generation. By combining photoinactive and photothermal effect, the nanoantenna array surface shows a more rapid inactivation compared to bare glass surface. Weibull model was utilized to analyze the inactivation kinetics of 405 nm exposure of *V. cholerae* on glass and nanoantenna surfaces. Compared to bare glass surface, results indicate that nanoantenna array surface exhibits a much higher germicidal efficiency by combining photoinactive and surface plasmonic enhanced photothermal effect. Live/Dead imaging was performed to validate the killing efficiency of 405 nm on nanoantenna surface after 20 min exposure.

Bibliography

1. Massad, G. and J.D. Oliver, *New selective and differential medium for Vibrio cholerae and Vibrio vulnificus.* Applied and Environmental Microbiology, 1987. **53**(9): p. 2262.
2. Maugeri, T.L., D. Caccamo, and C. Gugliandolo, *Potentially pathogenic vibrios in brackish waters and mussels.* Journal of Applied Microbiology, 2001. **89**(2): p. 261-266.
3. Oliver, J.D., L. Nilsson, and S. Kjelleberg, *Formation of nonculturable Vibrio vulnificus cells and its relationship to the starvation state.* Applied and Environmental Microbiology, 1991. **57**(9): p. 2640.
4. Jiang, X. and T.J. Chai, *Survival of Vibrio parahaemolyticus at low temperatures under starvation conditions and subsequent resuscitation of viable, nonculturable cells.* Applied and Environmental Microbiology, 1996. **62**(4): p. 1300.
5. Finkelstein, R.A. and J.C. Feeley, *Cholera.* CRC Critical Reviews in Microbiology, 1973. **2**(4): p. 553-623.
6. Yamamoto, T. and T. Yokota, *Electron microscopic study of Vibrio cholerae O1 adherence to the mucus coat and villus surface in the human small intestine.* Infection and Immunity, 1988. **56**(10): p. 2753.
7. Ali, M., et al., *Updated Global Burden of Cholera in Endemic Countries.* PLoS Neglected Tropical Diseases, 2015. **9**(6): p. e0003832.
8. Organization, W.H., *Cholerae.* (2011, January 5)

9. Pavlovsky, L., et al., *Effects of Temperature on the Morphological, Polymeric, and Mechanical Properties of Staphylococcus epidermidis Bacterial Biofilms.* Langmuir, 2015. **31**(6): p. 2036-2042.

10. Dijana, T., et al., *Diode Laser Irradiation in Endodontic Therapy through Cycles - in vitro Study.* Balkan Journal of Dental Medicine, 2017. **21**(2): p. 108-111.

11. Gill, J., et al., *Design of Laser Treatment Protocols for Bacterial Disinfection in Root Canals Using Theoretical Modeling and MicroCT Imaging.* Journal of Thermal Science and Engineering Applications, 2012. **4**(3): p. 031011-031011-9.

12. Tsen, K.T., et al., *Selective inactivation of micro-organisms with near-infrared femtosecond laser pulses.* Journal of Physics: Condensed Matter, 2007. **19**(47): p. 472201.

13. Sahu, G.K., R. Chowdhury, and J. Das, *Heat shock response and heat shock protein antigens of Vibrio cholerae.* Infection and Immunity, 1994. **62**(12): p. 5624.

14. Santos, G.M., et al., *Photothermal inactivation of heat-resistant bacteria on nanoporous gold disk arrays.* Optical Materials Express, 2016. **6**(4): p. 1217-1229.

15. Dai, T., et al., *Blue light for infectious diseases: Propionibacterium acnes, Helicobacter pylori, and beyond?* Drug Resistance Updates, 2012. **15**(4): p. 223-236.

16. Imran, A., et al., *Recent Patents on Light-Based Anti-Infective Approaches.* Recent Patents on Anti-Infective Drug Discovery, 2018. **13**(1): p. 70-88.

17. Dai, T., *The antimicrobial effect of blue light: What are behind?* Virulence, 2017. **8**(6): p. 649-652.

18. Morton, C.A., et al., *An open study to determine the efficacy of blue light in the treatment of mild to moderate acne.* Journal of Dermatological Treatment, 2005. **16**(4): p. 219-223.

19. Ashkenazi, H., et al., *Eradication of Propionibacterium acnes by its endogenic porphyrins after illumination with high intensity blue light.* FEMS Immunology & Medical Microbiology, 2003. **35**(1): p. 17-24.

20. Kawada, A., et al., *Acne phototherapy with a high-intensity, enhanced, narrow-band, blue light source: an open study and in vitro investigation.* Journal of Dermatological Science, 2002. **30**(2): p. 129-135.

21. Ganz, R.A., et al., *Helicobacter pylori in patients can be killed by visible light.* Lasers in Surgery and Medicine, 2005. **36**(4): p. 260-265.

22. Hamblin, M.R., et al., *Helicobacter pylori Accumulates Photoactive Porphyrins and Is Killed by Visible Light.* Antimicrobial Agents and Chemotherapy, 2005. **49**(7): p. 2822.

23. Lembo, A.J., et al., *Treatment of Helicobacter pylori infection with intra-gastric violet light phototherapy: A pilot clinical trial.* Lasers in Surgery and Medicine, 2009. **41**(5): p. 337-344.

24. Fukui, M., et al., *Specific-wavelength visible light irradiation inhibits bacterial growth of Porphyromonas gingivalis.* Journal of Periodontal Research, 2007. **43**(2): p. 174-178.

25. Feuerstein, O., N. Persman, and E.I. Weiss, *Phototoxic Effect of Visible Light on Porphyromonas gingivalis and Fusobacterium nucleatum: An In Vitro Study¶†.* Photochemistry and Photobiology, 2007. **80**(3): p. 412-415.

26. Ahmed, I., et al., *Recent Patents on Light-Based Anti-Infective Approaches.* Recent patents on anti-infective drug discovery, 2017.

27. Maclean, M., et al., *405 nm light technology for the inactivation of pathogens and its potential role for environmental disinfection and infection control.* Journal of Hospital Infection, 2014. **88**(1): p. 1-11.

28. Chebath-Taub, D., et al., *Influence of blue light on Streptococcus mutans re-organization in biofilm.* Journal of Photochemistry and Photobiology B: Biology, 2012. **116**: p. 75-78.

29. Protection, T.I.C.o.N.-I.R., *GUIDELINES ON LIMITS OF EXPOSURE TO ULTRAVIOLET RADIATION OF WAVELENGTHS BETWEEN 180 nm AND 400 nm (INCOHERENT OPTICAL RADIATION).* 2004. **87**(2): p. 171-186.

30. Kim, M.-J., et al., *Antibacterial effect and mechanism of high-intensity 405±5nm light emitting diode on Bacillus cereus, Listeria monocytogenes, and Staphylococcus aureus under refrigerated condition.* Journal of Photochemistry and Photobiology B: Biology, 2015. **153**: p. 33-39.

31. Govorov, A.O. and H.H. Richardson, *Generating heat with metal nanoparticles.* Nano Today, 2007. **2**(1): p. 30-38.

32. Baffou, G., R. Quidant, and C. Girard, *Heat generation in plasmonic nanostructures: Influence of morphology*. Applied Physics Letters, 2009. **94**(15): p. 153109.

33. Coppens, Z.J., et al., *Probing and Controlling Photothermal Heat Generation in Plasmonic Nanostructures.* Nano Letters, 2013. **13**(3): p. 1023-1028.

34. Khosravi Khorashad, L., et al., *Localization of Excess Temperature Using Plasmonic Hot Spots in Metal Nanostructures: Combining Nano-Optical Antennas with the Fano Effect.* The Journal of Physical Chemistry C, 2016. **120**(24): p. 13215-13226.

35. Ahmadivand, A., N. Pala, and D.Ö. Güney, *Enhancement of photothermal heat generation by metallodielectric nanoplasmonic clusters.* Optics Express, 2015. **23**(11): p. A682-A691.

36. Mancini, A., et al., *Thermoplasmonic Effect of Surface-Enhanced Infrared Absorption in Vertical Nanoantenna Arrays.* The Journal of Physical Chemistry C, 2018. **122**(24): p. 13072-13081.

37. Baffou, G., et al., *Photoinduced Heating of Nanoparticle Arrays.* ACS Nano, 2013. **7**(8): p. 6478-6488.

38. Meibom, K.L., et al., *Chitin Induces Natural Competence in Vibrio cholerae.* 2005. **310**(5755): p. 1824-1827.

39. Utada, A.S., et al., *Vibrio cholerae use pili and flagella synergistically to effect motility switching and conditional surface attachment.* Nature Communications, 2014. **5**: p. 4913.

40. Yildiz, F.H., et al., *Molecular analysis of rugosity in a Vibrio cholerae O1 El Tor phase variant.* Molecular Microbiology, 2004. **53**(2): p. 497-515.

41. Beyhan, S., et al., *Regulation of Rugosity and Biofilm Formation in Vibrio cholerae: Comparison of VpsT and VpsR Regulons and Epistasis Analysis of vpsT, vpsR, and hapR.* Journal of Bacteriology, 2007. **189**(2): p. 388.

42. McDonald, R.S., et al., *405 nm light exposure of osteoblasts and inactivation of bacterial isolates from arthroplasty patients&58; potential for new disinfection applications&63.* European Cells and Materials (ECM), 2013. **25**: p. 204-214.

43. McKenzie, K., et al., *Photoinactivation of Bacteria Attached to Glass and Acrylic Surfaces by 405 nm Light: Potential Application for Biofilm Decontamination.* Photochemistry and Photobiology, 2013. **89**(4): p. 927-935.

44. Bialka, K.L., A. Demirci, and V.M. Puri, *Modeling the inactivation of Escherichia coli O157:H7 and Salmonella enterica on raspberries and strawberries resulting from exposure to ozone or pulsed UV-light.* Journal of Food Engineering, 2008. **85**(3): p. 444-449.

45. Unluturk, S., et al., *Modeling inactivation kinetics of liquid egg white exposed to UV-C irradiation.* International Journal of Food Microbiology, 2010. **142**(3): p. 341-347.

46. van Boekel, M.A.J.S., *On the use of the Weibull model to describe thermal inactivation of microbial vegetative cells.* International Journal of Food Microbiology, 2002. **74**(1): p. 139-159.